Real space crystallography and defects in molecular crystals

WILLIAM JONES, JOHN O. WILLIAMS

Edward Davies Chemical Laboratories, University College of Wales, Aberystwyth, UK

An image plane technique of crystallographic analysis (real space crystallography) is shown to be particularly useful in studying defects in thin molecular crystals. Contrast in electron images from line defects is enhanced at bend contours and details of the interaction between the strain fields of dislocations and the bend contours give an indication of the Burgers vector. The shift in bend contours at coherent planar boundaries separating two orientationally related structures (as occur in martensitic transformations) is found to be directly related to a variation in deviation (excitation) parameter as a result of a change in the position of a particular reciprocal lattice point perpendicular to the electron beam. Observations are consistent with a previously suggested model for such a transformation in 1:8 dichloro-10-Me anthracene. In addition, dark-field images taken around a bend contour pole in anthracene provide evidence for the existence of forbidden reflections resulting from double diffraction in the space group $P2_{1/a}$.

1. Introduction

When investigating structural imperfections in solids by transmission electron microscopy it has been customary to study diffraction contrast effects in the electron image together with the details of the corresponding selected area diffraction patterns under well-defined orientational conditions. Recently, however, Steeds and co-workers [1, 2] have shown that equivalent information can be obtained by analysis of the electron image alone provided appropriate use can be made of the extensive distortion of thin specimens when exposed to the electron beam. Under such conditions of local bending and simultaneous changes in orientation (for a sample of given thickness) bend contours arise that map out areas of the crystal which obey a common Bragg diffraction condition.

In our recent electron-microscopic observations on organic, molecular crystals, we have found the technique of "real-space crystallography" convenient, particularly when seeking information about structural imperfections in these solids. In any electron microscopic investigation of such materials difficulties arise because of the sensitivity of the crystals to electron beam damage and it is customary to work with low beam currents. Even under such conditions lifetimes are of the order of a few

minutes so that the operations of specimen orientation and recording of images and diffraction patterns need be carried out rapidly and advantageously with the specimen at low temperatures [3]. Any technique that will reduce this time and expedite operation is likely to find wide applicability when studying such materials. In this communication we will show how real space crystallography yields information about line defects (e.g. dislocations) and planar defects (e.g. phase boundaries) in three types of aromatic molecular crystals.

2. Results and discussion

2.1. Line defects

Thin samples ($\sim$ 70 to 200 nm), suitable for electron microscopic observation can be grown from a $\sim$ 0.005 M solution of the aromatic compound in xylene by evaporation on the surface of clean water. A typical bright-field image for such a p-terphenyl crystal at room temperature is shown in Fig. 1. There we see that contrast from the dislocation network is pronounced only in regions intersected by the bend contours [5]. In other regions the dislocations, although clearly present, are only weakly diffracting. Contrast formation in close proximity to a prominent bend contour depends on a variation in the excitation parameter s and
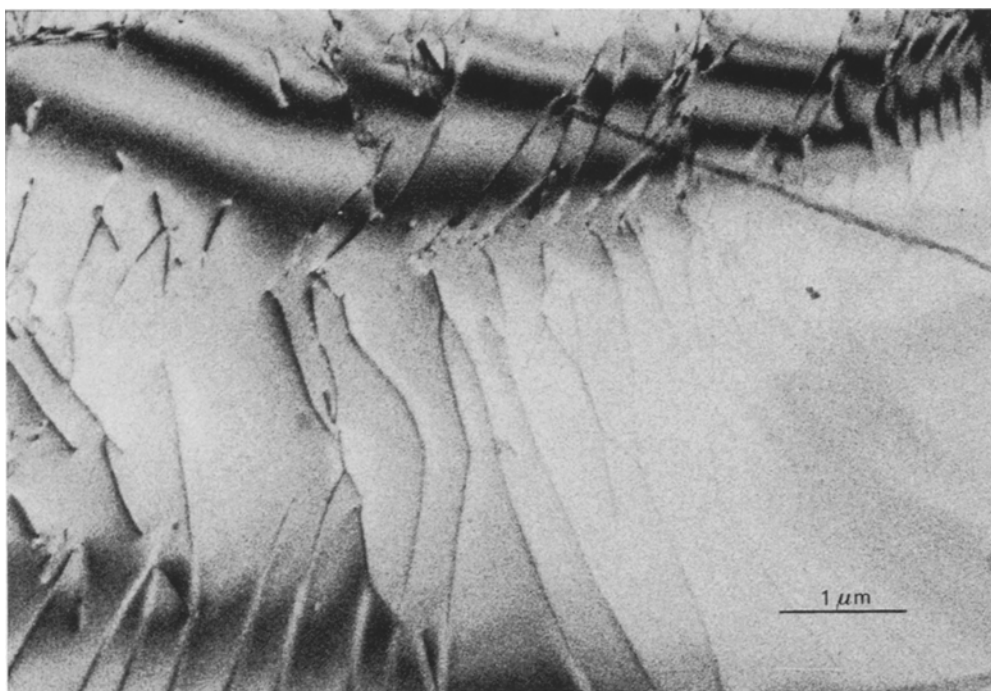
Figure 1 Bright-field electron micrograph of a *p*-terphenyl crystal showing dislocation networks in strong contrast in the vicinity of bend contours. Note the weak contrast in other regions.
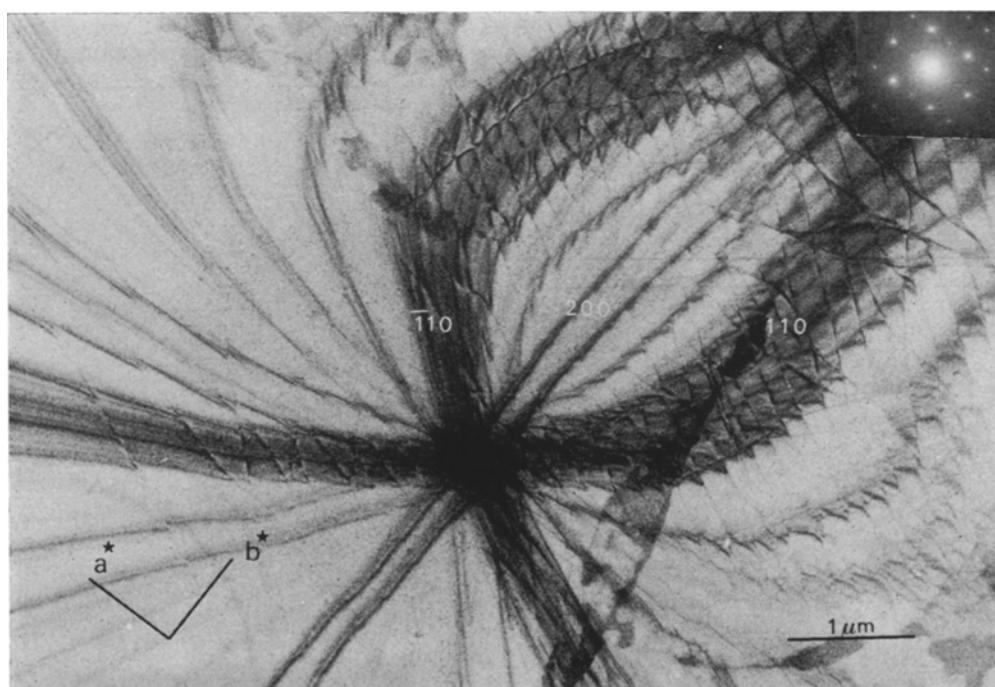

Figure 2 Bright-field electron micrograph of a *p*-terphenyl crystal showing a c^* bend contour pole (zone-axis pattern). The interaction between the bend contours and dislocations can be clearly seen.
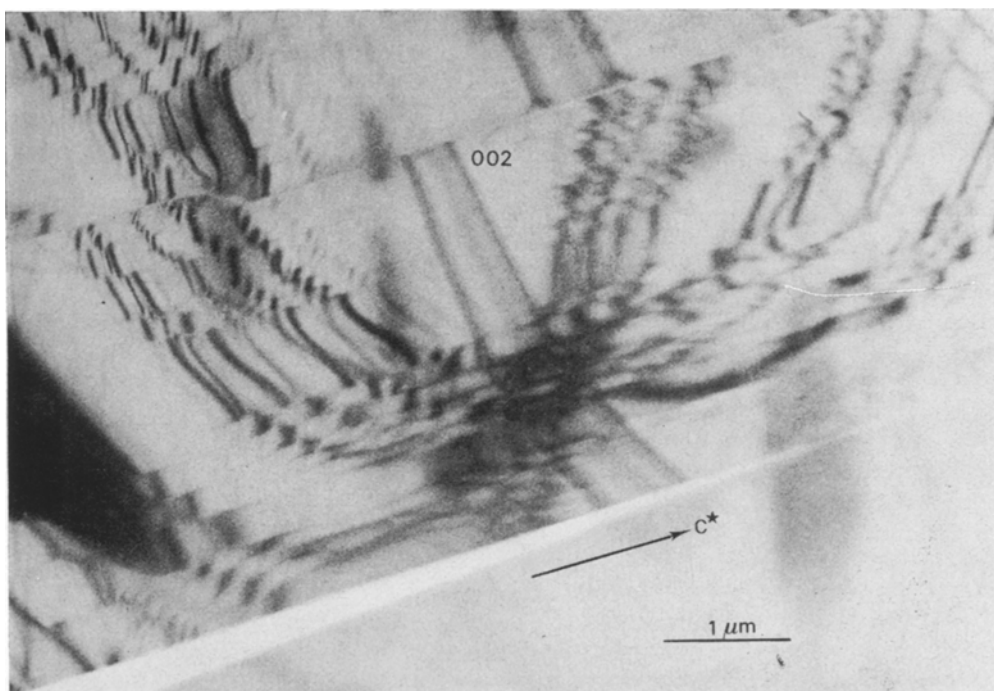
380

Figure 3 Bright-field electron micrograph of a 1:8 Cl_2-10-Me A crystal showing a [010] bend contour pole (zone-axis pattern). There is no apparent deviation of the 002 bend contour upon crossing the dislocations running in the c^* direction and the dislocation lines are not in contrast in this region.

has been discussed extensively elsewhere [4, 5].

The effect of lattice strains arising from imperfections is to cause local deviations of planes into and out of Bragg reflecting positions. In general, the strain field around dislocations produces no displacement of the diffracting planes if the Burgers vector lies parallel to these planes. Consequently, since bend contours indicate local regions of a crystal having common planes in reflecting positions their interaction with dislocations should give an indication of the Burgers vector of such faults. Ideally, therefore, if bend contours are to be utilized to ascertain Burgers vectors a dislocation network should be found and a bend contour pole (zone axis pattern) corresponding to a particular zone axis should, by appropriate sample tilting be set up in its vicinity. In this way the intersections of various (suitably indexed) bend contours with a given family of dislocations can then be examined. Fig. 2 shows such a bend contour pole corresponding to the c^* zone axis intersecting a dislocation network in a p-terphenyl crystal. The bend contours may be indexed and the assignment directly checked by reference to the selected-area diffraction pattern (see insert to Fig. 2)

and multiple dark-field images [5]. We see that the intensities of the bend contours are directly related to the intensities of the corresponding diffraction spots, and can be correlated with the structure amplitude of the particular reflection. The $hk0$ and $\bar{h}k0$ bend contour systems, in particular, are strongly perturbed by the dislocation network but the $h00$ system is hardly affected and the dislocations themselves are not imaged by this system indicating that the Burgers vector lies in [0 1 w] and is probably of the type [010]. In a similar way Fig. 3 shows a dislocation network intersecting a bend contour pole set up around the [010] zone axis in ortho-
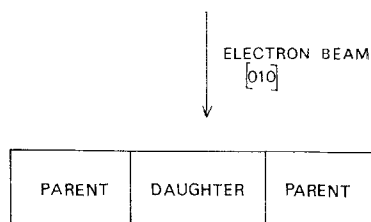

Figure 4 Schematic illustration showing the orientation of the sample surface and phase boundaries relative to the electron beam in 1:8 Cl_2-10-Me A.
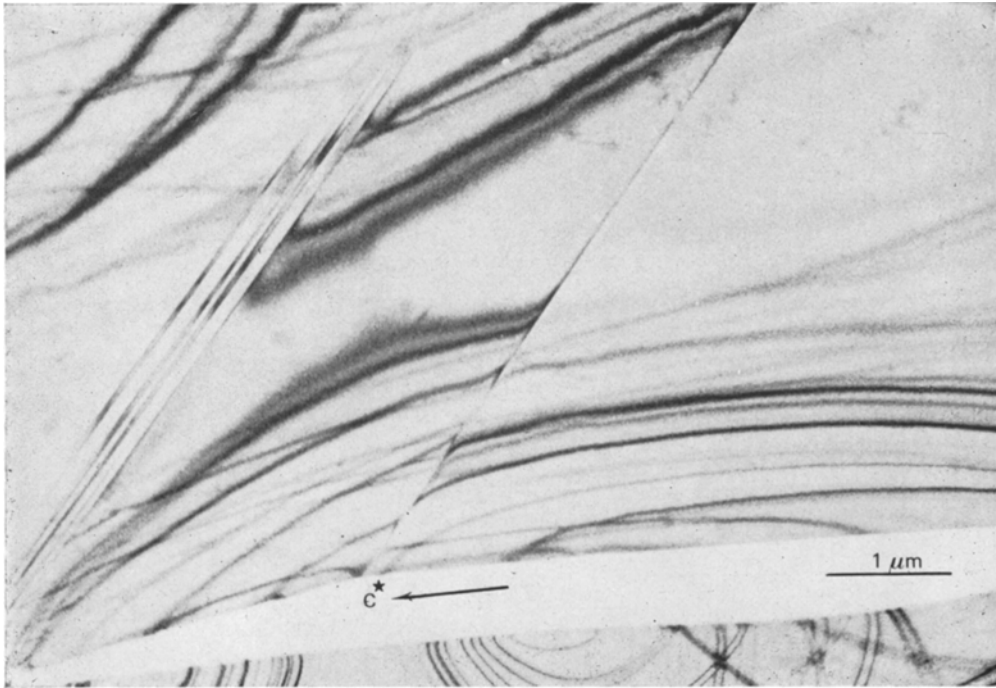
381

Figure 5 Bright-field electron micrograph of a 1:8 Cl_2-10-Me A crystal showing traces of the phase boundaries running approximately in a [1 0 3] direction.

rhombic ($P2_12_12_1$) 1:8 dichloro-10-methyl anthracene (1:8 Cl_2-10-Me A). In this case, the 0 0 2 bend contour is unaffected by the dislocation network running in [0 0 1]. The Burgers vector is likely to be [1 0 0]. The dislocations imaged in Fig. 3 are mainly edge in character and probably lie in planes normal to the electron beam.

2.2. Planar defects

Planar defects such as ferroelectric domains, Guinier-Preston zones, certain twin-lamellae and particular coherent boundaries need not have associated with them the extensive strain-fields usually accompanying linear and point defects. In such cases and especially when the boundaries are parallel to the electron beam the effect on bend contours in crossing planar faults can be evaluated. Contrast effects observed can be regarded as being produced by the geometry shown in Fig. 4 and the analysis is similar to the one developed by Goringe and Valdre [6] for the case of twins in V_3Si with boundaries parallel to the electron beam. It was shown that for such

boundaries the difference (δg) between corresponding reciprocal lattice points g_1 and g_2 (both with indices $hk0$) of the twinned regions is perpendicular to the boundary. Employing a reflecting sphere construction for a two-dimensional case Goringe and Valdre calculated the change in excitation parameter (s_g) caused by a change, δg, in the position of the reciprocal lattice point parallel to the foil surface, i.e. normal to the electron beam.*

Planar faults in 1:8 Cl_2-10-Me A have been observed and characterized by optical and electron microscopic techniques [7, 8]. They are interpreted as being due to a stress-induced phase transformation [9, 10] and an orientational relationship exists between the structures separated by the coherent, planar boundaries lying on twin related {2.88, 0, 1} invariant planes. There is a misorientation, ϕ, of approximately 8.5° between the (1 0 0) [and therefore also (0 0 1)] in the parent (P) and daughter (D) lattices. The {3 0 1} planes are parallel and have almost the same interplanar spacings in the two phases

---

*A more general expression, applicable to those cases in which the angle of misorientation of the crystal $\gamma \geqslant \theta$, the Bragg angle has been given by White [11].
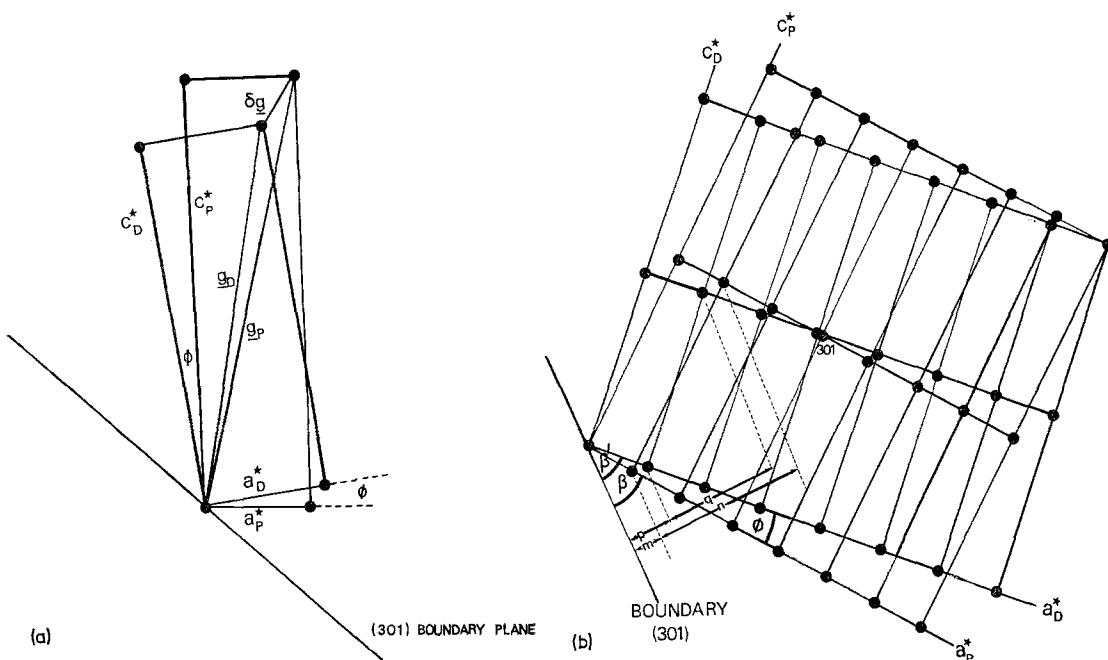
Figure 6 (a) Schematic illustration of the relationships between the a^*c^* reciprocal unit cells for the parent (P) and daughter (D) structures in 1:8 Cl_2-10-Me A. (b) Schematic illustration of the relative orientations of parent and daughter structures relative to traces of the (301) phase boundary. Note the correspondence of g_{702} and the near correspondence of g_{301} for both structures.

which are defined by the reciprocal lattice vectors $a_P^* = 0.0655$ Å^{-1}, $c_P^* = 0.2500$ Å^{-1} for the parent and $a_D^* = 0.0733$ Å^{-1}, $c_D^* = 0.2157$ Å^{-1} for the daughter lattices as found from selected-area diffraction photographs. According to the requirements [9, 10] of such diffusionless (martensitic) transformations the b^*-axis is invariant – a fact which is consistent with our experimental observations [7, 8].

It is possible to calculate the changes in excitation parameter s caused by a change, δg, in the position of a particular reciprocal lattice point defined by the vector g_P in the parent lattice to g_D in the daughter lattice. In the case of the planar boundaries in 1:8 Cl_2-10-Me A (see Fig. 5) the situation is simplified since the **g** vector of the operating reflection will have the same indices $(h0l)$ in the two phases, i.e. $g_P = (h0l)_P$ and $g_D = (h0l)_D$. The relationship between the reciprocal lattices of the two struc-

tures is schematically shown in Fig. 6a and the reciprocal lattice section drawn with respect to the normal to the (301) boundary plane given in Fig. 6b. Only approximate agreement between the calculated and experimental values of δs, the change in s_g, can be obtained in our case and the shifts in position of bend contours in crossing the phase boundary (see Fig. 7a) cannot be explained employing the equations developed by Goringe and Valdre [6] and White [11]. However, we may, in Fig. 7a, evaluate the orientation of the electron beam at various points along the phase boundary – a property defined by the vector k_{xz}. This vector directly relates the deviation of various parts of the crystal from Bragg orientations. For an orthorhombic structure the relationship between k_{xz} (u, v, w) and s_g for a particular reflection $g(h, k, l)$ may be written in the form

$$s_g = - \frac{\left[\left\{ \frac{(u+h)^2}{a^2} + \frac{(v+k)^2}{b^2} + \frac{(w+l)^2}{c^2} \right\} - \left\{ \frac{u^2}{a^2} + \frac{v^2}{b^2} + \frac{w^2}{c^2} \right\} \right]}{2K}$$

(1)

where a, b and c are the lattice constants and $K = 1/\lambda$ (λ is the electron wavelength which under our operating conditions of 100 keV is 0.037 Å). At the bend contours which demarcate Bragg oriented regions of the crystal $s_g = 0$ and substitution of the appropriate values of h, k, l and a, b, c into Equation 1 yield the values of k_{xz} at these points e.g. k_{xz} corresponding to positions of the $h00$ and $\bar{h}00$ bend contours are $\dfrac{h}{2}00$ and $\dfrac{h}{2}00$ respectively. Furthermore, midway between a pair of bend contours (e.g. see Fig. 7b) $k_{xz} = 0$ and the appropriate value of s_g can be found. The relevant values of s_g, k_{xz} and k_{xz} for the bend contours corresponding to the vectors $g_P{}^i$ and labelled in Fig. 7a are given in Table I. Knowing the transformation matrix that relates $g_P{}^i$ and $g_D{}^i$ and assuming that the electron beam orientation in the parent and daughter phases is the same at the boundary we may check whether $s_{gD}{}^i = 0$ at the value of k_{xz} predicted by the position of the bend contour in the daughter region. For the main bend contour systems interacting with the phase boundary shown in Fig. 7a values of B/A as shown in Table I are calculated which are in good agreement with the observed direction and magnitude of the shift in the bend contours. Consequently, it may be concluded that close examination of variations in bend contour patterns across phase boundaries are in quantitative agreement with electron diffraction data.
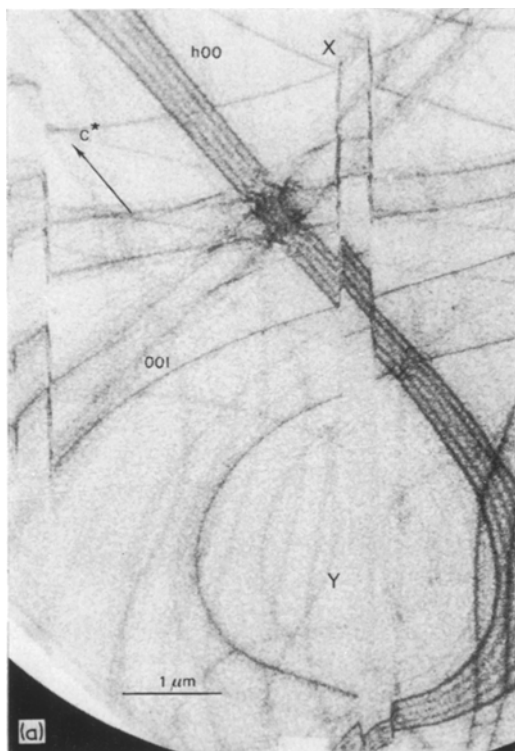
2.3. Forbidden reflections and double diffraction

Owing to the multiple scattering of electrons which occurs even in very thin crystals, diffraction spots can appear in positions that are normally forbidden from symmetry considerations. Anthracene belongs to the space group $P2_{1/a}$ and so $0k0$ reflections with k odd and
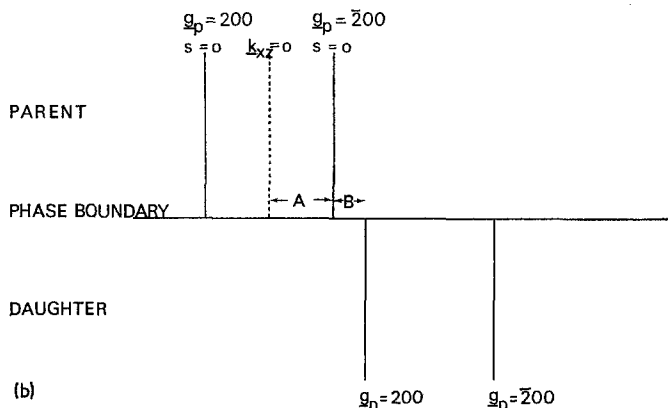

Figure 7 (a) Bright-field electron micrograph showing the interaction of bend contours emanating from a 010 pole with a region of the daughter phase within the parent matrix. Note the shifts in the $h00$ and $00l$ bend contour systems at the phase boundary XY. (b) Schematic illustration of the relative shift (B/A) in the $h00$ bend contour system across the phase boundary. At the bend contours the excitation parameter $s = 0$ since at this point the planes are in the exact Bragg reflecting position.
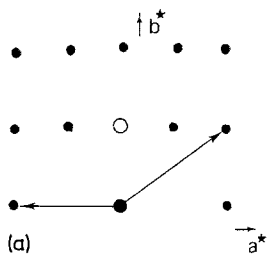
Figure 8 (a) Schematic diagram of the a^*b^* reciprocal lattice section of p-terphenyl indicating the symmetry forbidden "reflections" at 100, $\bar{1}$00 and 010. Double diffraction, however, causes spots to appear at these positions e.g. 0 at 010 according to the vectorial addition indicated. (b) Dark-field electron micrograph about a c^* pole in p-terphenyl corresponding to the "forbidden reflection" 010 circled in (a). (c) Dark-field electron micrograph of the same pole as in (b) taken with a symmetry allowed 210 reflection.
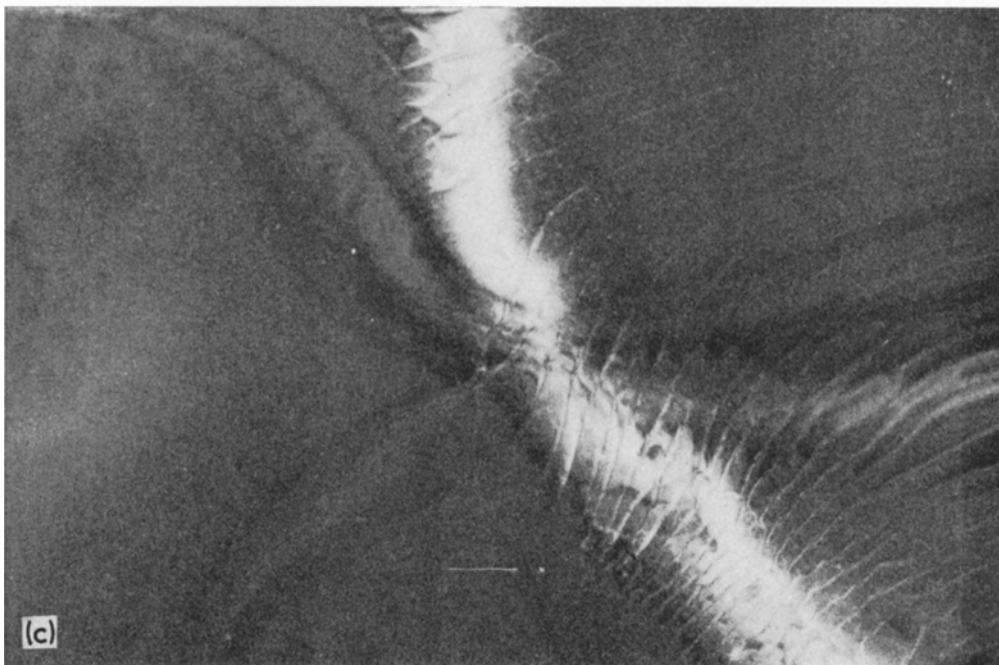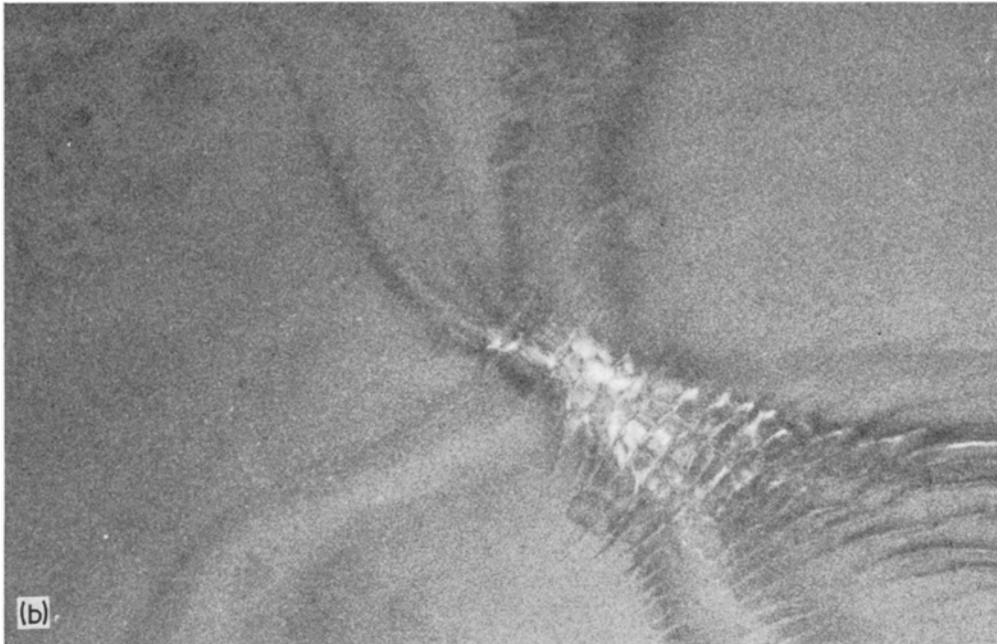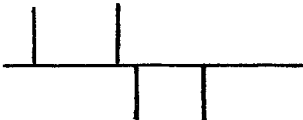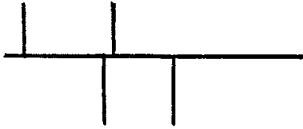
TABLE I

Bend contour	k_{xz} at $s_g = 0$	k_{xz}	s_g at $k_{xz} = 0$ for g_P^i (Å^{-1})	B/A calculated	Nature of shift (observed).
100_P	$\bar{\tfrac{1}{2}}00$	0.032	0.000 08	$\tfrac{1}{8}$	Forbidden
$\bar{1}00_P$	$\tfrac{1}{2}00$	0.032			reflection
100_D	$\bar{\tfrac{1}{2}}00$	0.036			
001_P	$00\bar{\tfrac{1}{2}}$	0.062	0.001 4	$\tfrac{1}{8}$	Forbidden
$00\bar{1}_P$	$00\tfrac{1}{2}$	0.062			reflection
001_D	$00\tfrac{1}{2}$	0.054			
200_P	$\bar{1}00$	0.065	0.000 32	$\tfrac{1}{8}$	
$\bar{2}00_P$	100	0.065			
200_D	$\bar{1}00$	0.073			
002_P	$00\bar{1}$	0.125	0.004 5	$\tfrac{1}{8}$	
$00\bar{2}_P$	001	0.125			
002_D	$00\bar{1}$	0.108			
101_P	$\bar{\tfrac{1}{2}}0\bar{\tfrac{1}{2}}$	0.07	0.000 15	$\tfrac{1}{10}$	
$\bar{1}0\bar{1}_P$	$\tfrac{1}{2}0\tfrac{1}{2}$	0.07			
101_D	$\bar{\tfrac{1}{2}}0\bar{\tfrac{1}{2}}$	0.065			

$h0l$ reflections when h is odd should be absent. However, in a diffraction pattern (see Fig. 8a) taken with the electron beam incident along c^*, spots invariably appear in these forbidden positions. Fig. 8b is a dark-field electron micrograph taken by encircling the reflection occurring in the 0 1 0 position (circled in Fig. 8a) and shows that strong diffraction is limited to the region of the zone axis confirming that double diffraction does indeed occur. A bend contour at a pole taken in dark-field employing an allowed reflection, 2 1 0, is shown for comparison in Fig. 8c. A similar situation holds for p-terphenyl and the "forbidden" reflections are clearly seen in the insert diffraction pattern of Fig. 2.

Acknowledgements

References

1. J. W. STEEDS, G. J. TATLOCK and J. HAMPSON, *Nature (Lond.)* **241** (1973) 435.
2. G. J. TATLOCK and J. W. STEEDS, *ibid* **246** (1973) 126.
3. W. JONES, J. M. THOMAS, J. O. WILLIAMS and L. W. HOBBS, *J. Chem. Soc. Faraday Trans.* II, in press.
4. G. THOMAS, in "Transmission Electron Microscopy of Metals" (Wiley, New York, 1962) p. 51.
5. L. B. HIRSCH, A. HOWIE, R. B. NICHOLSON, D. W. PASHLEY and M. J. WHELAN, "Electron Microscopy of Thin Crystals" (Butterworths, London, 1965) p. 304.
6. M. J. GORINGE and U. VALDRE, *Proc. Roy. Soc.* **295** (1966) 192.
7. J. O. WILLIAMS, *J. Mater. Sci.* **8** (1973) 1361.
8. W. JONES, J. M. THOMAS and J. O. WILLIAMS, to be published.
9. M. BEVIS and E. B. CRELLIN, *Polymer* **12** (1971) 666.
10. P. ALLAN, E. B. CRELLIN and M. BEVIS, *Phil. Mag.* **27** (1973) 127.
11. J. R. WHITE, *J. Mater. Sci.* **10** (1975) 541.